

Fig. 3. The variation in the $\Delta\sigma$, σ_{300} , and percent hematite components as a function of annealing time for samples annealed at 900°C (Fig. 1).

on x-ray. Furthermore, the northeastern Alberta sample has a practically constant magnetization between 200° and 600°C and a large amount of hematite (23 percent), whereas all the other type 2 samples have a linear decrease in magnetization with temperature between 220° and 500°C and between 5 and 10 percent hematite. The (220) spinel reflection of varying intensity is present in x-ray for all the thermally treated nontronites in Table 1 except the northeastern Alberta nontronite. This peak is strongest in the Hemet and Riverside samples. Magnetic and detailed x-ray analysis of the thermally treated Hemet nontronite suggests that the type 1 behavior is due to this spinel phase, which is possibly maghemite, with a Curie temperature of 540°C (8).

The correlation between the presence of cristobalite and type 2 σ - T behavior is convincing. Although we do not have direct evidence for the existence of "magnetic cristobalite," it seems that the phase responsible for the 4.1-Å reflection is also responsible for type 2 magnetic behavior. A spinel phase, possible maghemite, is probably the type 1 component. Identification of the type 1 phase as a spinel is also consistent with the σ - T analysis (Fig. 3): prolonged annealing transforms this spinel to hematite. It is also clear from Table 1 that the crystallization of quartz rather than cristobalite inhibits the formation of the type 2 phase.

At this juncture we speculate that the type 2 phase is cristobalite, either iron-substituted or doped. Both the HF experiment and the negative correlation between the relative amounts ($\Delta\sigma$) of the type 2 phase produced and the appearance of quartz support this interpretation. If most of the SiO₂ in the original nontronite lattice is recrystallizing as quartz, then there will be less silica available to produce "iron-cristobalite." It is

also intriguing that cristobalite is reported to undergo a displacive transition from the α -form (tetrahedral) to the β -form (cubic) between 180° and 280°C (9); this transition may be responsible for the apparent T_c at 220°C. On this hypothesis the α -form is (ferri?)magnetic, whereas the β -form is antiferromagnetic or paramagnetic. A mixture of α -Fe₂O₃ and colloidal SiO₂ in molar proportions equivalent to nontronite was annealed at 1550°C in the stability field of cristobalite (9) for 24 hours. X-ray analysis revealed only cristobalite, Fe₃O₄, and α -Fe₂O₃, but magnetic measurements showed that no type 2 phase was produced. Possibly the formation of magnetic cristobalite at 900° to 1000°C requires topotactic growth from a smectite precursor.

Although we do not yet have an adequate explanation for the field cooling experiments (Fig. 2), they do suggest that their ultimate cause may be exchange anisotropy (10). This exchange

anisotropy could be produced by the interaction between the type 1 and type 2 phases or by the interactions between ferromagnetic and antiferromagnetic regions produced by compositional fluctuations within the type 2 phase alone. Further research is needed to resolve this uncertainty.

BRUCE M. MOSKOWITZ
ROBERT B. HARGRAVES

Department of Geological and
Geophysical Sciences,
Princeton University,
Princeton, New Jersey 08544

References and Notes

1. B. M. Moskowitz and R. B. Hargraves, *J. Geophys. Res.* **87**, 10 (1982).
2. P. Toulmin III *et al.*, *ibid.* **82**, 4625 (1977).
3. C. Allen, J. L. Gooding, M. Jercinsvic, K. Keil, *Icarus* **45**, 347 (1981); A. Banin and L. Margulies, *Nature (London)* **305**, 523 (1983).
4. R. B. Hargraves, D. W. Collinson, R. E. Arvidson, C. R. Spitzer, *J. Geophys. Res.* **82**, 4547 (1977); R. B. Hargraves, D. W. Collinson, R. E. Arvidson, P. M. Cates, *ibid.* **84**, 8379 (1979).
5. P. F. Kerr *et al.*, *Am. Pet. Inst. Res. Proj.* **49**, (Report No. 7) (1951).
6. B. M. Moskowitz and R. B. Hargraves, *Eos* **63**, 310 (1982).
7. R. J. D. Mackenzie and E. D. Rogers [*Thermochim. Acta* **18**, 177 (1977)] claimed that maghemite was produced by the thermal decomposition of their nontronite samples.
8. If the type 1 phase is maghemite, then the maghemite exhibits very high stability with heating. In (7) it was suggested that this was due to the presence of silicon in the maghemite structure.
9. W. A. Deer, R. A. Howie, J. Zussman, *Rock-Forming Minerals* (Wiley, New York, 1963), vol. 4, p. 343.
10. W. H. Meiklejohn and C. P. Bean, *Phys. Rev.* **105**, 904 (1957).
11. W. Petruk, D. M. Eirrell, E. E. Lavier, R. J. Tremblay, P. G. Manning, *Can. Mineral* **15**, 14 (1977).
12. We thank C. Lawson and S. K. Banerjee for helpful discussions and critical comments. We thank R. Stallard, F. B. Van Houten, and A. K. Baird who contributed samples of nontronite. This work was supported by NASA grant NAGW-372.

27 February 1984; accepted 12 June 1984

Remote Acoustic Imaging of the Plume from a Submarine Spring in an Arctic Fjord

Abstract. *Acoustic backscatter observations at 200 kilohertz were made of the buoyant plume from a submarine spring at a depth of 47 meters in Cambridge Fiord, Baffin Island. Vertical velocities of up to 37 centimeters per second are inferred from the ascent rates of discrete scattering structures in the plume.*

A plume of brackish water has been observed rising from a submarine spring at a depth of 47 m on the prodelta at the head of Cambridge Fiord, Baffin Island. The observations were made from a 10-m launch during September in 1982 and 1983, and include 200-kHz acoustic backscatter images of the plume and conductivity-temperature-depth (CTD) and vertical velocity profiles (1). These results appear to be novel and to have useful implications for the monitoring of

buoyant plumes in the marine environment in general.

The discharge of ground water through the sea floor has only recently become a focus for research, and most known points of outflow occur in water shallow enough for the plume to rise to the surface (2). Evidence has been presented, however, suggesting that such discharge occurs at depths as great as 500 m on the Florida continental slope (3) and that ground water seepage on the conti-

mental slope of the eastern United States was a factor in the development of submarine canyons (4). The study of isolated point sources of buoyancy at these water depths with conventional oceanographic instrumentation is difficult. The purpose of this report is to describe potential advantages of using acoustic remote sensing techniques in such studies.

The submarine spring in Cambridge Fiord was discovered (5) because it results in the annual formation of a polynya in late March. The source of fresh water for the spring appears to be a nearby lake, and the fresh water discharge from the spring has been estimated to be $0.14 \text{ m}^3/\text{sec}$ from the 2-m wintertime decrease in the level of the lake (5). The present study was conducted during the ice-free season, and there was no surface manifestation of the spring's existence. The location of the polynya in winter (5) was used to position a marker float, and the plume was located by making low-speed acoustic sounding transects in the vicinity of the marker with a 200-kHz portable acoustic sounder (Ross Laboratories) (6).

A typical acoustic image obtained in this fashion is shown in Fig. 1a. The plume extends from the bottom at a depth of about 47 m to a minimum depth of 9 m. Plume width increases with height above bottom, and there is some indication that between 12 and 20 m the plume is spreading horizontally, although the acoustic backscatter amplitude decreases rapidly with distance from the plume axis. The horizontal scale of this image is not known, although results to be discussed later show that at 33 m the plume is about 8 m wide.

Figure 1b shows an image of the plume obtained 1 year later while the launch was held approximately stationary over the vent by a four-point mooring. Discrete scattering structures rise from the bottom at approximately constant speeds and then decelerate above 25 m. Maximum ascent rates are 22 to 37 cm/sec, as inferred from the slopes of the straight-line trajectories in the 25- to 45-m depth interval. The echo from the CTD instrument (Guildline model 8770) during three descents and two ascents can also be seen in Fig. 1b in the 0- to 10-m depth interval. Backscatter from the plume masks this echo at greater depths.

Temperature, salinity, and density anomaly (σ_t) profiles (Fig. 2a), corresponding to the first ascent of the CTD instrument, exhibit large-amplitude fine structure beginning at 10 m (the top of the plume in the acoustic image in Fig.

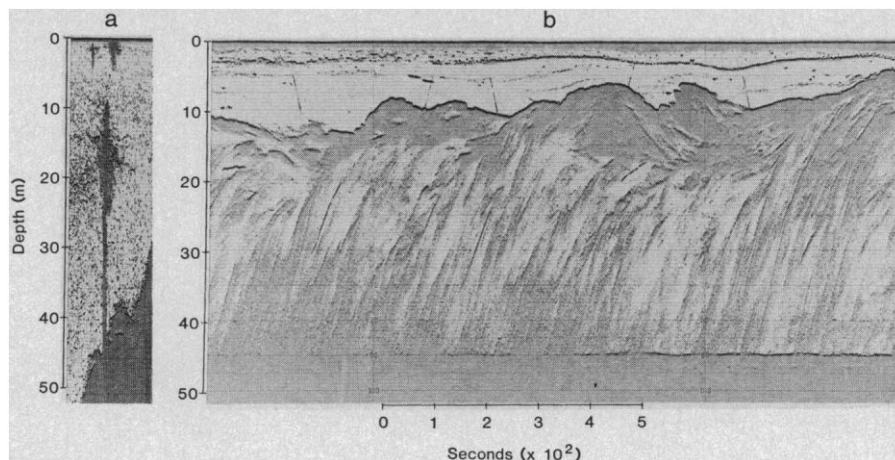


Fig. 1. Acoustic backscatter images of the buoyant plume, obtained (a) in September 1982 while steaming slowly over the vent and (b) in September 1983 while moored over the vent.

1b) and extending to the bottom. Note the absence of water of very low salinity: the minimum observed salinities are ~ 30.8 per mil. Profiles of the same quantities (Fig. 2b) at a location removed from, but close to, the vent site exhibit fine structure of lower amplitude confined to a low-temperature core in the 15- to 24-m depth interval. Temperatures at depths below 32 m decrease on average toward the bottom, but do not reach 0°C and are warmer (by as much as 0.4°C) in the profiles taken over the vent. Below 20 m salinities are consistently lower (by up to 0.2 per mil) over the vent. Also presented in Fig. 2b (as a dashed line) is the temperature profile obtained on the following day at a location about 100 m from the vent, showing that the upper mixed layer in this fjord is warmer (1.5°C) than the deep water ($< -0.5^\circ\text{C}$). These vertical profiles indicate that cold, brackish water is advected upward in the plume. This is confirmed by the horizontal temperature profile through the plume at a depth of 33 m in Fig. 2c, from which the plume width is also observed to be about 8 m. The low-temperature core and associated fine structure at 15 to 24 m in Fig. 2b are caused by lateral spreading of the plume along isopycnal surfaces.

Direct measurements of vertical velocity were made in the plume with a direct-reading acoustic current meter (Neil Brown Instrument Systems) at a depth of 10 m. These measurements ranged from 7 to 18 cm/sec at a time when the acoustic scattering structures were observed to rise almost to the surface and are consistent with the observed rates of ascent of these structures. This suggests that vertical velocities in the plume can be inferred directly from the slopes of the scattering structure trajectories.

These results can be compared with the theory of buoyant plumes (7, 8). Because the observations were made at the head of the fjord during calm conditions shortly before freeze-up, a time of essentially no runoff, and because the tidal range is small (less than 1 m), the ambient current speeds are expected to be low and the plume to be axisymmetric. The latter expectation is to some extent confirmed by acoustic images similar to that in Fig. 1a and corresponding to acoustic sounding transects in different directions over the vent. None of these images exhibit pronounced asymmetry, and in all cases the plume cap is well above the neutrally buoyant, horizontally spreading part of the plume, an effect that is most pronounced for buoyant plumes symmetrical about the vertical axis (7, 8).

Order of magnitude estimates can be made of the discharge characteristics at the vent. From the acoustic image in Fig. 1b, vertical velocity (U_0) at the vent and terminal height of rise of the plume above bottom are determined to be 35 cm/sec and 37 m, respectively. Given the definitions of density defect $\Delta = (\rho_0 - \rho_1)/\rho_0$ and lateral scale $b_0 = D/2$ in terms of the densities ρ_1 and ρ_0 within and outside the jet at vent level and the vent diameter D , the terminal plume height and the momentum and volume fluxes can be written in nondimensional form (7, 8): $\xi_t = 0.368 b_0^{-1/2} \Delta^{-1/4}$, $m_0 = 1.57 \times 10^{-8} \Delta^{-2}$, and $\mu_0 = 6.79 \times 10^{-4} b_0^{1/2} \Delta^{-3/4}$, respectively. The buoyancy frequency in the ambient fluid was taken to be 6.2×10^{-3} per second (Fig. 2b) and the entrainment constant and square root of the turbulent Schmidt number to be 0.082 and 1.16. Since m_0 is independent of initial jet width, a unique solution can be obtained

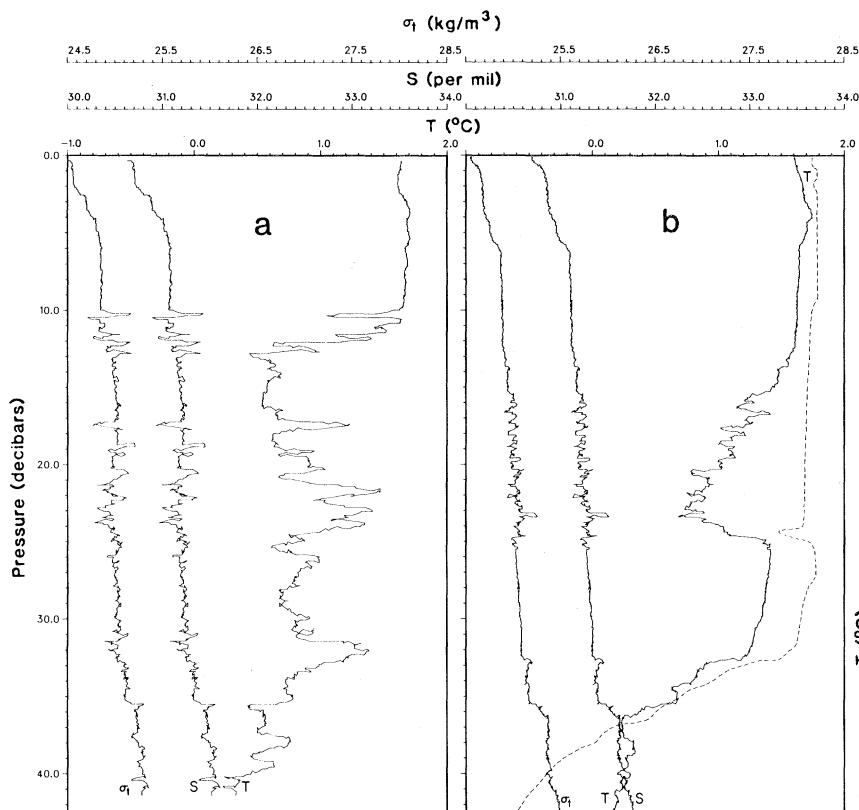


Fig. 2. Temperature (T), salinity (S) and density anomaly (σ_t) profiles. (a) Vertical profiles corresponding to Fig. 1b. (b) Vertical profiles at a location near the vent site, obtained about 30 minutes before those in (a). Also shown is a temperature profile obtained on the following day (dashed line). (c) Horizontal temperature profile through the plume at a depth of 33 m. Closed circles represent the mean; broken lines connect the minimum and maximum temperatures observed at each CTD position.

for a given value of Δ by using the numerical results in figure 12 of Fan and Brooks (7), yielding estimates of b_0 and μ_0 . Applying the additional constraint that the volume discharge $Q_0 = \pi D^2 U_0 / 4$ be within an order of magnitude of $0.14 \text{ m}^3/\text{sec}$ (5), it is found that for $\Delta = 10^{-4}$, $b_0 > 4.2 \text{ m}$ and Q_0 is too large ($>9.6 \text{ m}^3/\text{sec}$); for $\Delta = 10^{-2}$, m_0 is very small, $\xi_t \approx 2.82$ —the value for a simple plume—and Q_0 is small ($\sim 0.016 \text{ m}^3/\text{sec}$); but for $\Delta = 10^{-3}$, a solution exists ($b_0 = 0.79$, $\xi_t = 2.33$, and $\mu_0 = 1.08$) for which $Q_0 = 0.34 \text{ m}^3/\text{sec}$, which is acceptable and which gives $D = 1.1 \text{ m}$. Because density is controlled by salinity at these temperatures, the salinity at the vent should be about 1 per mil less than ambient salinity, or 30.9 per mil (Fig. 2b). This is consistent with minimum observed salinities (~ 30.8 per mil) in the plume but requires that the fresh water mix with seawater in the prodelta before discharge. This is possible, given the porous nature of the gravelly delta sediments.

The maximum height of rise is very sensitive to the vertical density gradient in the surrounding fluid. The oscillations in plume height in the acoustic image in Fig. 1b have periods typical of internal waves (>2.5 minutes) and may arise from changes in ambient stratification induced by internal waves. Such changes also occur at lower frequencies due to internal tides or in response to changing

winds; the dashed-line temperature profile in Fig. 2b illustrates altered stratification of this type (since the pycnocline and thermocline are roughly coincident). The cold water at the depth of the vent raises the possibility of ice formation in the plume. Because of the associated change in volume and the high acoustic impedance of ice relative to water, ice crystals could contribute significantly to the buoyancy flux and to the backscattered acoustic signal. Given the temperature and salinity profiles in Fig. 2, a and b, however, it is unlikely that ice crystals were present when the acoustic image in Fig. 1b was obtained. This implies that small-scale differences in temperature and salinity associated with turbulent mixing in the plume, or with instabilities at the plume edge, may be responsible for the observed backscatter. This is partially supported by the rapid lateral decay of backscatter intensity (Fig. 1a) and by the decreased fine structure amplitudes in the laterally spreading, neutrally buoyant plume (Fig. 2b), consistent with the diminished turbulence intensities expected in this zone. Other scatterers, such as organisms or suspended particulates, must also be considered, however,

In summary, these results demonstrate that buoyant plumes from submarine springs are readily detected by high-frequency acoustic remote-sensing techniques and that it may be possible to

estimate vertical velocities directly from the rate of rise of discrete scattering structures in the plume. The nature of these scattering structures and the scattering mechanisms are not well understood but may be related to turbulence and instabilities in the plume.

ALEX E. HAY

Department of Physics and NICOS,
Memorial University of Newfoundland,
St. John's, Newfoundland,
Canada A1B 3X7

References and Notes

1. A. E. Hay, *Eos* **64**, 1022 (Abstr.) (1983); *Can. Data Rep. Hydrogr. Ocean Sci. No. 12* (1983), pp. 7-1-7-4.
2. F. A. Kohout, paper presented at the Symposium on Hydrology and Water Resources Development, Ankara, Turkey, 7 to 12 February 1966.
3. F. T. Manheim, *Trans. N.Y. Acad. Sci.* **29**, 839 (1967).
4. J. M. Robb, *Geology* **12**, 278 (1984).
5. H. E. Sadler and H. V. Serson, in *Fjord Oceanography*, H. J. Freeland, D. M. Farmer, C. D. Levings, Eds. (Plenum, New York, 1980), pp. 299-304.
6. A. E. Hay, *J. Geophys. Res.* **88**, 7525 (1983).
7. L.-N. Fan and N. H. Brooks, *Calif. Inst. Technol. Rep. No. KH-R-18* (1969).
8. E. J. List, *Annu. Rev. Fluid Mech.* **14**, 189 (1982); K. Hofer and K. Hutter, *J. Non-Equilib. Thermodyn.* **6**, 49 (1981).
9. I thank J. P. M. Syvitski and C. T. Schafer, the crew of C.S.S. *Hudson*, and J. Banner, J. Foley, R. Trites, and U. Weyer for assistance in the field; L. Petrie for CTD data reduction; and the Department of Oceanography, University of British Columbia, for the use of the sounder. Supported by the Natural Sciences and Engineering Research Council, Canada, and the Department of Energy, Mines, and Resources, Canada. This is Sedimentology of Arctic Fjords Experiment contribution No. 3 and Newfoundland Institute for Cold Ocean Science contribution No. 50.

16 February 1984; accepted 25 June 1984